



## OPEN

# The ClC-3 chloride channel associated with microtubules is a target of paclitaxel in its induced-apoptosis

SUBJECT AREAS:  
TARGET IDENTIFICATION  
CHLORIDE CHANNELS  
APOPTOSIS  
ION TRANSPORT

Haifeng Zhang<sup>1,2\*</sup>, Huarong Li<sup>3,6\*</sup>, Lili Yang<sup>3</sup>, Zhiqin Deng<sup>1</sup>, Hai Luo<sup>1,5</sup>, Dong Ye<sup>3,5</sup>, Zhiqian Bai<sup>1</sup>, Linyan Zhu<sup>3</sup>, Wencai Ye<sup>4</sup>, Liwei Wang<sup>1</sup> & Lixin Chen<sup>3</sup>

Received  
8 March 2013

Accepted  
20 August 2013

Published  
12 September 2013

Correspondence and requests for materials should be addressed to W.Y. (chywc@yahoo.com.cn); L.W. (twangliwei@jnu.edu.cn) or L.C. (chenlixinw@sohu.com)

\* These authors contributed equally to this work.

<sup>1</sup>Department of Physiology, Medical College, Jinan University, Guangzhou 510632, China, <sup>2</sup>Department of Pathology, School of Medicine, Xi'an Jiaotong University, Xi'an 710061, China, <sup>3</sup>Department of Pharmacology, Medical College, Jinan University, Guangzhou 510632, China, <sup>4</sup>College of Pharmacy, Jinan University, Guangzhou 510632, China, <sup>5</sup>Department of Pathophysiology, Medical College, Jinan University, Guangzhou 510632, China, <sup>6</sup>Guangdong Province Key Laboratory of Molecular Immunology and Antibody Engineering, Jinan University, Guangzhou 510632, China.

Recent evidences show that cationic fluxes play a pivotal role in cell apoptosis. In this study, the roles of Cl<sup>-</sup> channels in paclitaxel-induced apoptosis were investigated in nasopharyngeal carcinoma CNE-2Z cells. Chloride current and apoptosis were induced by paclitaxel and inhibited by chloride channel blockers. Paclitaxel-activated current possessed similar properties to volume-activated chloride current. After ClC-3 was knocked-down by ClC-3-siRNA, hypotonicity-activated and paclitaxel-induced chloride currents were obviously decreased, indicating that the chloride channel involved in paclitaxel-induced apoptosis may be ClC-3. In early apoptotic cells, ClC-3 was up-regulated significantly; over-expressed ClC-3 was accumulated in cell membrane to form intercrossed filaments, which were co-localized with  $\alpha$ -tubulins; changes of ultrastructures and decrease of flexibility in cell membrane were detected by atomic force microscopy. These suggest that ClC-3 is a critical target of paclitaxel and the involvement of ClC-3 in apoptosis may be associated with its accumulation with membrane microtubules and its over activation.

Cancer has been a leading cause of death worldwide. The development of cancer is a multi-step process, which is triggered by carcinogens (chemicals, ultraviolet, ionizing radiation and tumor virus, etc.), controlled by various mechanisms (oncogenes, tumor suppressor genes, apoptosis-regulatory genes, DNA repair genes, signaling molecules, transcription factors, inflammation factors and telomeres, etc.), and associated with the background of heredity. In addition to surgery and radiotherapy, chemotherapy is a common tool used to wipe carcinoma cells off patients.

Paclitaxel is one of the most successful and broadest-spectrum anticancer agents. It is currently used in the treatment of patients with ovarian and breast carcinoma and is also effective in the treatment of cancer of lung, head and neck, bladder, and esophageal origins<sup>1,2</sup>. Although much work has been done, the exact action mechanisms of paclitaxel on cancer have not yet been clarified. Paclitaxel can combine with microtubules and causes assembly of microtubules, resulting in the arrest of the cell cycle at the mitotic phase. It has also been found that paclitaxel can activate the release of cytotoxic cytokines, cyclin-dependent kinases and c-Jun N-terminal kinases/stress-activated protein kinases to promote apoptosis. In addition, paclitaxel has been shown to regulate apoptosis at the transcriptional level. Resistance to paclitaxel can be developed in cancer patients and may be associated with Tau proteins<sup>3</sup>. These discoveries indicate that paclitaxel initiates apoptosis through multiple mechanisms. A better elucidation of the mechanisms underlying the paclitaxel-induced apoptosis may facilitate the treatment of cancer.

Apoptosis is a multi-step and multi-pathway cell death program, which is controlled by a diverse range of cell signals<sup>4</sup>. A defined feature of apoptosis in all cells is the apoptotic volume decrease (AVD), which has been considered to be a hallmark of the early stage of apoptosis and an early prerequisite to apoptosis<sup>5-8</sup>. Although debates are existed, there is no doubt that ionic fluxes play a pivotal role in AVD and the volume-sensitive Cl<sup>-</sup> channel has been highly regarded<sup>9-14</sup>.

ClC-3, a member of the ClC superfamily of voltage-gated chloride channels, is widely expressed and hypothesized as a volume-sensitive Cl<sup>-</sup> channel. Some data suggest that ClC-3 could modulate the apoptosis induced by H<sub>2</sub>O<sub>2</sub>, thapsigargin, ischemia/reperfusion and transforming growth factor (TGF)-beta<sup>15-18</sup>.



Although paclitaxel is used as a compelling chemotherapeutic drug, there is no much knowledge about the function of chloride channels in paclitaxel-induced apoptosis. In this study, the roles of chloride channels in the paclitaxel-induced apoptosis and changes in the ultrastructure of the cell membrane were investigated in the poorly differentiated nasopharyngeal carcinoma CNE-2Z cells.

## Results

**Paclitaxel induced apoptosis in CNE-2Z cells.** Apoptotic cells were detected by the double-staining (Annexin V-FITC and propidium iodide) technique, following the protocol shown in the methods. Based on the principles of this technique, the normal cells were not stained by the two dyes (Annexin V-FITC<sup>-</sup>/PI<sup>-</sup>); the early apoptotic cells could only be dyed by Annexin V-FITC (Annexin V-FITC<sup>+</sup>/PI<sup>-</sup>); the late apoptotic cells were positive in both Annexin V-FITC and PI staining (Annexin V-FITC<sup>+</sup>/PI<sup>+</sup>).

Cells were bathed in the control RPMI 1640 medium with or without paclitaxel for 3–6 h, and then were stained with Annexin V-FITC (green) and propidium iodide (PI, red). As shown in Fig. 1A, most control cells were not stained, indicating that the apoptotic rate was very low in the control group. In the cells treated with 10  $\mu$ M paclitaxel for 3 h, most cells were stained by Annexin V-FITC (green), but not by PI, indicating that most of the paclitaxel-treated cells were in the early apoptotic stage. In the cells exposed to 10  $\mu$ M paclitaxel for 6 h, some were stained by both dyes, indicating that these cells were in the late apoptotic stage. Further analysis showed that 3 h after the paclitaxel treatment,  $70.02 \pm 0.93\%$  of cells had stepped into the early apoptotic stage (3 experiments,  $P < 0.01$ , vs control; Fig. 1B), but the percentage of paclitaxel-treated cells in the late apoptotic stage was not significantly different from that in the control group ( $P > 0.05$ ). In those treated with paclitaxel for 6 h,  $53.19 \pm 6.47\%$  of the cells were in the early apoptotic stage and  $17.01 \pm 1.24\%$  were in the late stage ( $P < 0.01$ , vs control; 3 experiments).

The survivals of CNE-2Z cells treated with 0.1  $\mu$ M paclitaxel were also observed. In those treated with 0.1  $\mu$ M paclitaxel for 3 h, the early apoptotic cells were hardly detected. At 6 h, the early apoptotic cells began to appear, but the percentage of apoptotic cells was far less than that in the group treated with 10  $\mu$ M paclitaxel (data not shown).

Caspase-3, as an inactive zymogen in cells, is a key protease that is cleaved and activated during the early stage of apoptosis by extrinsic and intrinsic pathways. The cleaved caspase-3 is thus regarded as a marker of early apoptosis<sup>19–21</sup>. Here the cleaved caspase-3 (Asp175) was detected by confocal immunofluorescence in the control CNE-2Z cells and in the cells treated with 10  $\mu$ M paclitaxel for 3 h. The cleaved caspase-3-immunofluorescent images (cy-3, red) were shown in Fig. S1. Most of the paclitaxel-treated cells were positive in cleaved caspase-3-immunofluorescence. Analysis of the images indicated that  $64.20 \pm 3.10\%$  of the cells (three experiments) were in the early apoptotic stage, which was not significantly different from that detected by Annexin V-FITC ( $P > 0.05$ ).

**Paclitaxel activated Cl<sup>-</sup> currents in CNE-2Z cells.** Evidences presented by others and us suggest that ion channels including chloride channels may be involved in apoptosis<sup>22–25</sup>. The above data indicated that paclitaxel could induce apoptosis in CNE-2Z cells. The effects of paclitaxel on Cl<sup>-</sup> channels were investigated. As illustrated in Fig. 2, paclitaxel (10  $\mu$ M) activated a current in a few minutes. The current was almost completely inhibited by the cell shrinkage induced by exposure of cells to the 47% hypertonic bath solution ( $93.14 \pm 3.49\%$  at +80 mV,  $95.72 \pm 3.78\%$  at -80 mV,  $n = 10$ ), suggesting that the current is volume-sensitive (Fig. 2A). Extracellular application of the chloride channel blockers NPPB (100  $\mu$ M) and DIDS (100  $\mu$ M) suppressed the paclitaxel-activated current (Fig. 2B–D), but the inhibitory efficiency of the hypertonic

solution and NPPB ( $87.84 \pm 1.06\%$  at +80 mV,  $86.69 \pm 2.20\%$  at -80 mV,  $n = 10$ ) was higher than that of DIDS ( $53.32 \pm 3.98\%$  at +80 mV,  $21.56 \pm 5.14\%$  at -80 mV,  $n = 10$ ,  $P < 0.01$ ). The inhibitory effects of the hypertonic solution and NPPB did not depend on the voltages applied, but those of DIDS were voltage-dependent. The inhibitory efficiency at +80 mV was not significantly different from that at -80 mV in the hypertonic and NPPB groups ( $P > 0.05$ ), but was higher than that at -80 mV in the DIDS group ( $P < 0.01$ ). The current was reversed at a potential ( $-4.55 \pm 2.22$  mV,  $n = 15$ ) close to the equilibrium potential for Cl<sup>-</sup> (-0.9 mV), and displayed mild outward rectification, but did not show obvious voltage- or time-dependent inactivation (Fig. 2E–I). These results indicate that paclitaxel can activate a current, which is volume-sensitive and is mediated mainly by Cl<sup>-</sup> channels.

The effects of paclitaxel on chloride channels were also tested at a lower concentration (0.1  $\mu$ M, Fig. 2F). The results showed that 0.1  $\mu$ M paclitaxel could also activate a chloride current with the properties similar to those activated by 10  $\mu$ M paclitaxel, but the current density ( $46.92 \pm 7.69$  pA/pF, at +80 mV,  $n = 13$ ) was smaller than that activated by 10  $\mu$ M paclitaxel ( $67.85 \pm 0.83$  pA/pF, at +80 mV,  $P < 0.01$ ).

**The chloride channel blocker NPPB prevented the apoptosis induced by paclitaxel.** As shown above, paclitaxel could activate a chloride current in CNE-2Z cells, which was blocked by NPPB, suggesting that activation of chloride channels may be an important event in paclitaxel-induced apoptosis. To confirm this postulation, the effects of Cl<sup>-</sup> channel blockers on apoptosis of CNE-2Z cells induced by paclitaxel were investigated. As shown in Fig. S2 and Table 1, incubation of cells in the medium containing paclitaxel (10  $\mu$ M) alone for 3 h or 6 h induced significantly cell apoptosis; most of the cells stepped into the early stage of apoptosis. NPPB (100  $\mu$ M) alone did not show significant effects on cell survival ( $P > 0.05$ , vs control). However, addition of NPPB in the medium prevented or inhibited the paclitaxel-induced apoptosis. The percentage of apoptotic cells (including the apoptotic cells in early and late stages) was decreased from about 70% (paclitaxel alone) to 4.5% (paclitaxel plus NPPB) (three experiments,  $P < 0.01$ ). These results suggest that the activation of chloride channels may be a key event in the paclitaxel-induced apoptosis of CNE-2Z cells.

**The ClC-3 chloride channel was a target of paclitaxel.** It was reported by us previously, that hypotonicity-induced cell swelling activated a Cl<sup>-</sup> current in CNE-2Z cells<sup>26,27</sup>. We found in this study that the paclitaxel-activated Cl<sup>-</sup> current was volume-sensitive, and shared similar properties with the hypotonicity-activated Cl<sup>-</sup> current. Consistent with the hypotonicity-activated Cl<sup>-</sup> current, the paclitaxel-activated Cl<sup>-</sup> current not only possessed the properties of linear conductance, negligible time-dependent inactivation, weak outward rectification and volume-sensitivity, they also had similar reversal potentials and could be blocked by NPPB (Fig. S3).

ClC-3 is considered as a candidate of volume-sensitive Cl<sup>-</sup> channels. In this study, the role of ClC-3 in the activation of the paclitaxel-activated Cl<sup>-</sup> current was studied. The expression of ClC-3 proteins in CNE-2Z cells was knocked down by small interfering RNA (siRNA). As presented in Fig. 3A, ClC-3-siRNAs conjugated with 5'-FAM (green) were transfected successfully into CNE-2Z cells. Analysis of the transfected cells with the flow cytometry indicated that the transfection efficiency was about 90%. The expression of ClC-3 proteins was significantly decreased by 48 h treatment with ClC-3-siRNA (3 experiments,  $P < 0.05$ ), but the treatment of cells with the negative control siRNA (NC-siRNA) did not show significant effect on ClC-3 expression (Fig. 3B, C).

The chloride currents in the control cells and in the cells successfully transfected with 5'-FAM conjugated siRNA (marked by green fluorescence) were recorded with the patch clamp technique under the fluorescence microscope. The results indicated that the

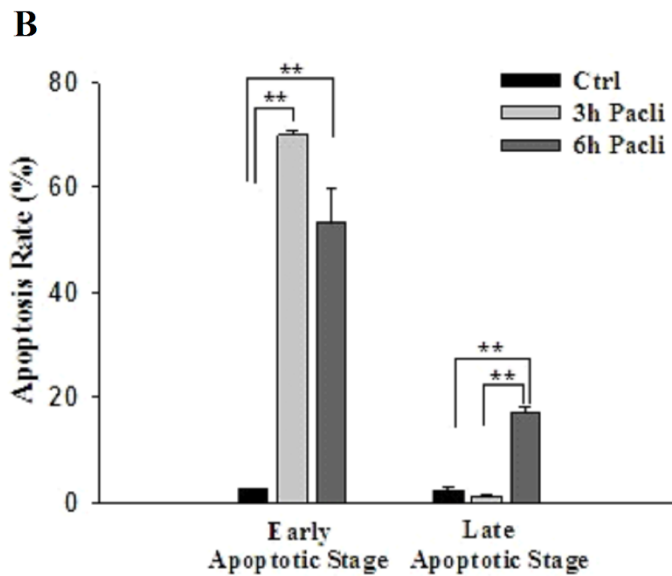
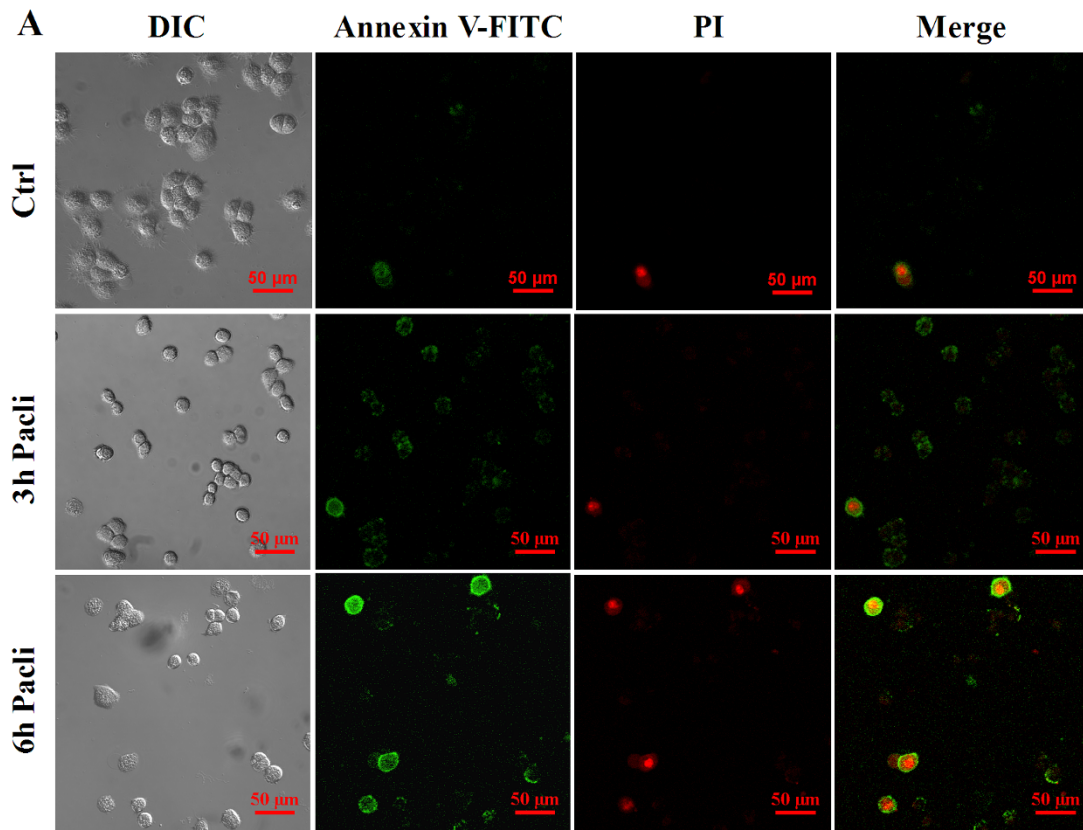


**Figure 1 | Paclitaxel-induced apoptosis of CNE-2Z cells detected by the Annexin V-FITC/PI double staining assay.** CNE-2Z cells were treated with 10  $\mu\text{M}$  paclitaxel for 3 h or 6 h (3 h or 6 h Pacli), stained with Annexin V-FITC (green) and propidium iodide (PI, red), and detected by the confocal microscopy. (A) shows the representative images, and (B) presents the percentage of cells in early and late stages of apoptosis obtained by analysis of the cell images (mean  $\pm$  SE, 3 experiments). **DIC**, the images obtained by differential interference contrast microscopy; **Merge**, the merged images of Annexin V-FITC and PI images; **Ctrl**, control cells; \*\*,  $P < 0.01$ .

knockdown of ClC-3 expression attenuated the activation of the hypotonicity-activated and paclitaxel-activated  $\text{Cl}^-$  currents. As illustrated in Fig. 3D–G, paclitaxel hardly induced a current, and hypotonic challenges just activated a small current in the cells successfully transfected with ClC-3-siRNA. The paclitaxel-activated  $\text{Cl}^-$  current in the ClC-3-siRNA group was  $5.65 \pm 1.10$  pA/pF at +80 mV ( $n = 5$ ), which was significantly lower than that in the control group

( $67.85 \pm 0.83$  pA/pF,  $n = 3$ ,  $P < 0.01$ ) and that in the negative control siRNA group ( $64.81 \pm 4.00$  pA/pF,  $n = 5$ ,  $P < 0.01$ ) (Fig. 3G). The hypotonicity-activated  $\text{Cl}^-$  current in the ClC-3-siRNA group was also lower than that in the control and negative control siRNA groups ( $P < 0.01$ , Fig. 3F). These results suggest that ClC-3 may be the main chloride channel protein mediating the apoptosis of CNE-2Z cells induced by paclitaxel.

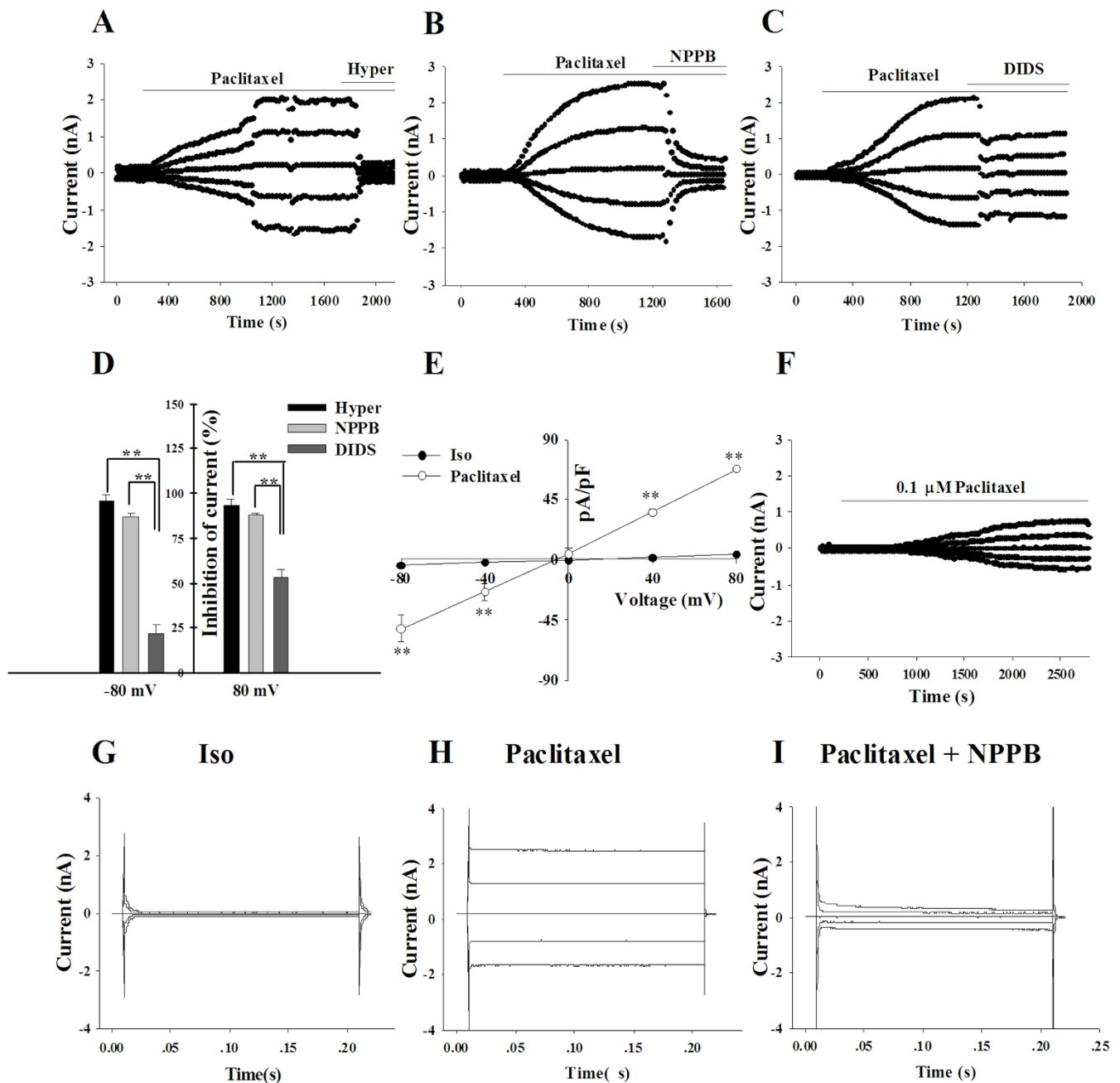


**Figure 2** | Activation of chloride currents by paclitaxel in CNE-2Z cells. (A), (B) and (C) are the typical time courses of activation of  $\text{Cl}^-$  currents by  $10 \mu\text{M}$  paclitaxel and inhibition of the currents by the 47% hypertonic challenge (Hyper),  $100 \mu\text{M}$  NPPB and  $100 \mu\text{M}$  DIDS, respectively. (D) presents the inhibitions of paclitaxel-activated  $\text{Cl}^-$  currents by the hypertonic solution, NPPB and DIDS (mean  $\pm$  SE,  $n = 10$ ,  $** P < 0.01$ ). (E) shows the I-V relationship of the paclitaxel-activated  $\text{Cl}^-$  current (mean  $\pm$  SE,  $n = 15$ ,  $** P < 0.01$ , vs Iso). (F) is the typical time courses of activation of  $\text{Cl}^-$  currents by  $0.1 \mu\text{M}$  paclitaxel. (G), (H) and (I) are the typical current traces recorded in the isotonic solution (Iso) and in the isotonic solution containing paclitaxel or paclitaxel plus NPPB, respectively. Cells were held at  $0 \text{ mV}$  and stepped to  $0, \pm 40$  and  $\pm 80 \text{ mV}$  repeatedly.

**Table 1** | Inhibition of paclitaxel-induced apoptosis by the chloride channel blocker NPPB in CNE-2Z cells (Mean  $\pm$  SE,  $n = 3$ )

Group	Early Apoptotic Stage (%)	Late Apoptotic Stage (%)
<b>Control</b>	$2.60 \pm 0.18$	$2.36 \pm 0.52$
<b>3 h NPPB</b>	$1.26 \pm 0.34$	$1.08 \pm 0.20$
<b>6 h NPPB</b>	$1.02 \pm 0.27$	$2.03 \pm 0.27$
<b>3 h Paclitaxel</b>	$70.02 \pm 0.93$	$1.31 \pm 0.37$
<b>3 h NPPB + Paclitaxel</b>	$28.22 \pm 4.24^{**}$	$3.00 \pm 1.07$
<b>6 h Paclitaxel</b>	$53.19 \pm 6.47$	$17.01 \pm 1.24$
<b>6 h NPPB + Paclitaxel</b>	$2.46 \pm 0.89^{**}$	$2.09 \pm 0.25^{**}$

$**P < 0.01$  (3 h NPPB + Paclitaxel vs 3 h Paclitaxel, 6 h NPPB + Paclitaxel vs 6 h Paclitaxel).

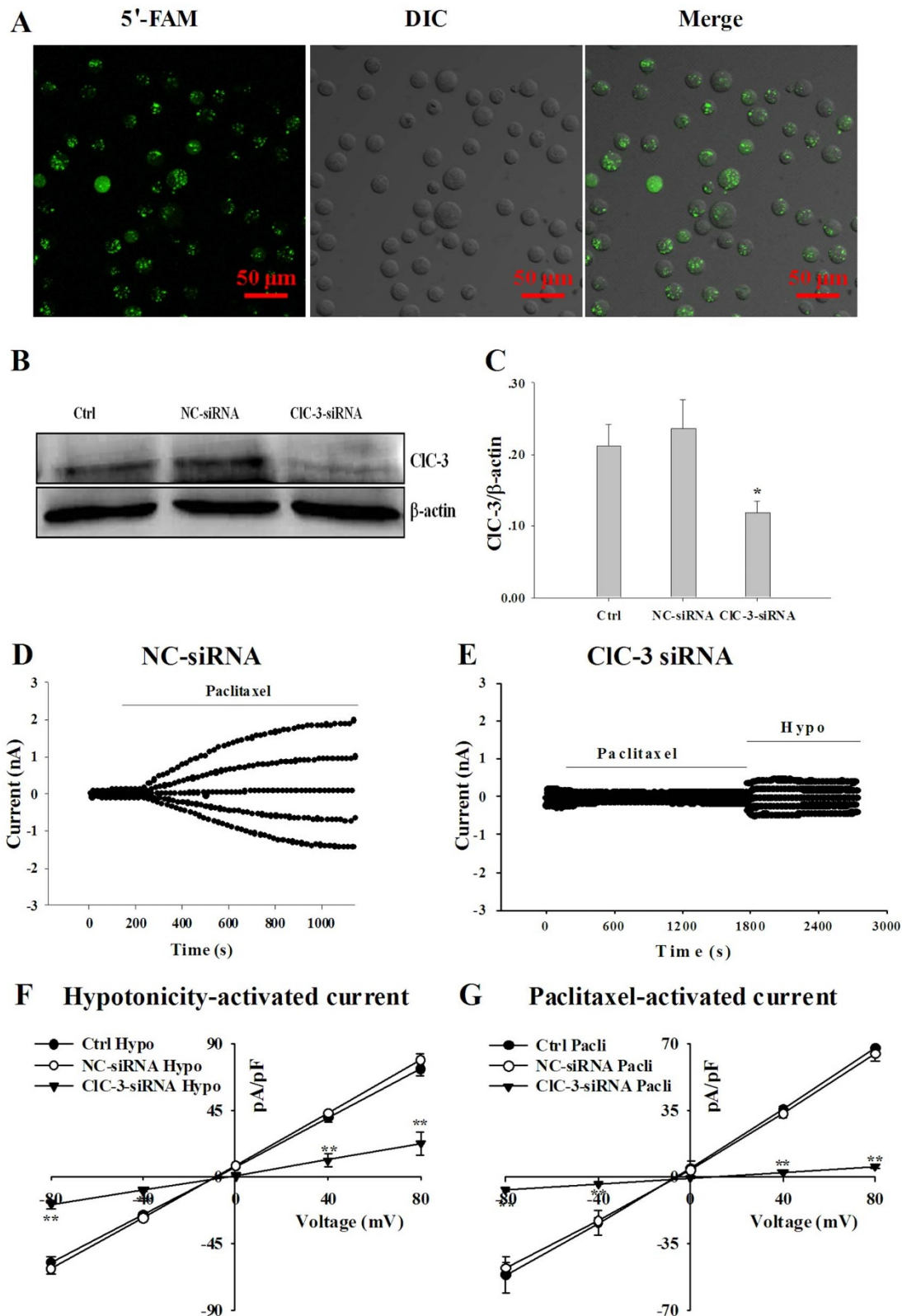


**Figure 3** | Inhibition of CIC-3 protein expression and paclitaxel-activated chloride currents by CIC-3 siRNA in CNE-2Z cells. (A) shows the CNE-2Z cells transfected with 5'-FAM-labeled siRNA (Green) and detected by the confocal microscopy. (B) and (C) present the knock-down expression of CIC-3 proteins by CIC-3 siRNA, but not by the negative control siRNA (NC-siRNA), detected by Western blotting analysis (mean  $\pm$  SE, 3 experiments under the same conditions; \*  $P < 0.05$ , vs control). (D) and (E) are the typical time courses of paclitaxel (10  $\mu$ M)-induced  $\text{Cl}^-$  currents in cells treated with the negative control siRNA and CIC-3 siRNA, respectively. (F) and (G) show hypotonicity-activated and paclitaxel-induced  $\text{Cl}^-$  currents under different conditions at 0,  $\pm 40$  and  $\pm 80$  mV, respectively (mean  $\pm$  SE of 3 to 10 cells).



**CIC-3 protein expression and distribution were changed in the early stage of apoptosis induced by paclitaxel.** CIC-3 protein expression was measured in the early apoptotic stage of CNE-2Z cells. As presented in Fig. S4, the CIC-3 protein expression in the CNE-2Z cells incubated with 10  $\mu$ M paclitaxel for 3 h was increased significantly. The expression level in paclitaxel-treated cells was 2.3 and 1.8 folds of that in the control group detected by immunofluorescence and the Western blotting assay, respectively.

CIC-3 subcellular localization was analyzed by immunofluorescent 3D images. 3D images were obtained by reconstructing all X-Y transverse section images, which were scanned every 0.25  $\mu$ m along Z axis under the confocal microscope with 100  $\times$  oil lens, using the Nikon NIS-Elements AR software. As shown in Fig. 4, CIC-3 proteins were labeled with cy-3 (red) and the nuclei were stained by DAPI (blue). Green cubes represented the portion

reserved when others were moved away. In control group, CIC-3 proteins were distributed in the entire cell as shown in the whole-cell image (Ctrl whole), but mainly in the cell membrane, plasma and nuclei as shown in the crest image (Ctrl crest, the bottoms of cells were cut off) and in the bottom image (Ctrl bottom, the tops of cells were cropped away). In the cells treated with 10  $\mu$ M paclitaxel for 3 h (Pacli), CIC-3 proteins were distributed and clustered in the cells as presented in the whole-cell image (Pacli whole). After the bottoms of cells were taken off, the crest image (Pacli crest) displayed that CIC-3 proteins were accumulated in the cell membrane to form filaments, which intercrossed like a bird nest. In the bottom image (Pacli bottom), in which the tops of cells were cut off, CIC-3 proteins formed similar filaments as in the crest image. The 3D movies of the control and paclitaxel-treated cells were displayed in Supplementary movie 1 and Supplementary movie 2 in the supplement, respectively.

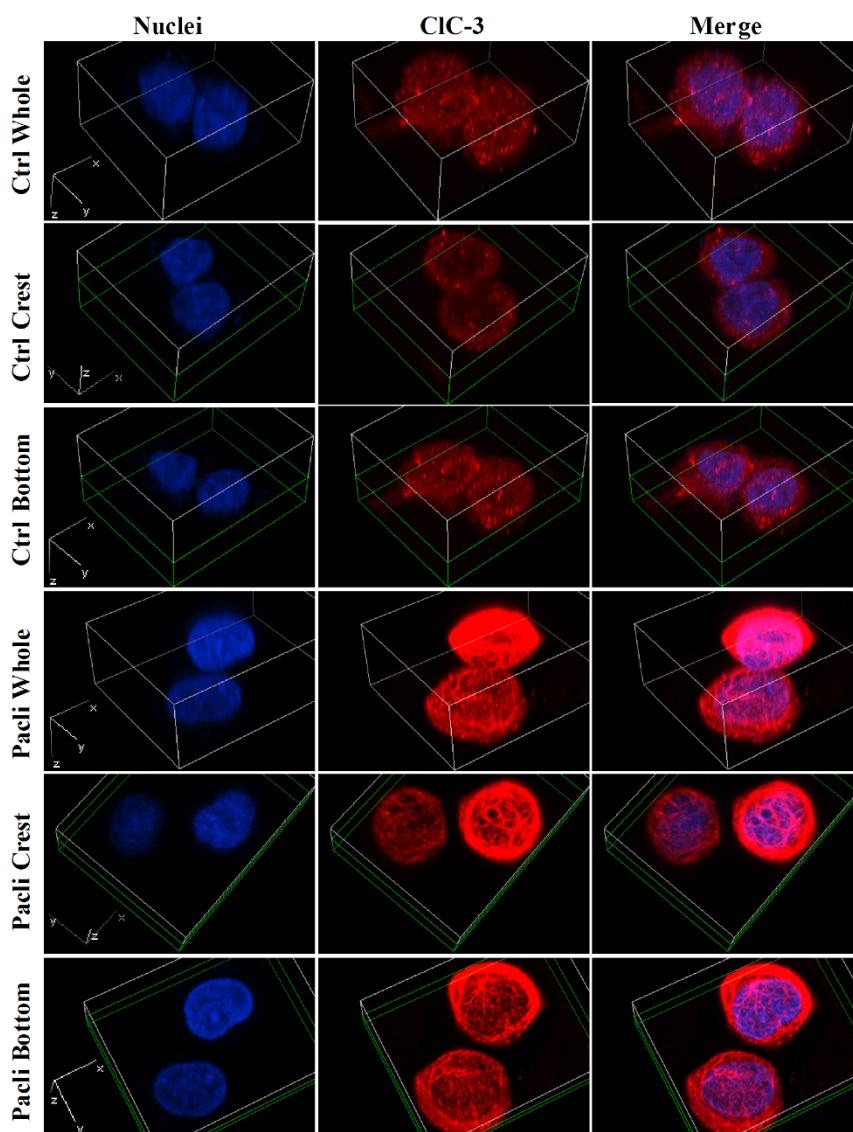


**Figure 4** | Effects of paclitaxel on subcellular localization of CIC-3 proteins in CNE-2Z cells. CIC-3 proteins were detected by immunofluorescence and labeled with cy-3 (red). The nuclei were stained by DAPI (blue). In control group, CIC-3 proteins are distributed over the entire cell (*Ctrl whole*); with the bottoms of the cells cut off, the control crest image shows that CIC-3 proteins primarily localize in the cell membrane and plasma (*Ctrl crest*); with the tops of the cells chopped away, the control bottom image presents that CIC-3 proteins localize in the cell membrane, plasma and nuclei (*Ctrl bottom*). In the cells treated with 10  $\mu$ M paclitaxel for 3 h (*Pacli*), CIC-3 proteins are distributed and clustered in the cells, and are accumulated in the cell membrane to form filaments, which intercross like a bird nest, as shown in the whole cell (*Pacli whole*), crest (*Pacli crest*) and bottom (*Pacli bottom*) images. Green cubes represent the portion reserved when others are removed. The 3D movies of the control and paclitaxel-treated cells were displayed in Supplementary movie 1 and Supplementary movie 2 in the supplement, respectively.



**CIC-3 proteins were co-localized with tubulins in the early apoptotic stage of CNE-2Z cells induced by paclitaxel.** As shown above, CIC-3 proteins were clustered in the cell membrane and formed intercrossed filaments after CNE-2Z cells were treated with 10  $\mu$ M paclitaxel for 3 h. Paclitaxel can selectively combine with microtubules and cause the assembly of microtubules. The microtubule disrupter colchicine inhibits PC2 channel activity, whereas the microtubular stabilizer paclitaxel increases PC2 channel activity<sup>28,29</sup>. In this study, the relationship between tubulin and CIC-3 in distribution was investigated.

As presented in Fig. 5, in control CNE-2Z cells, the  $\alpha$ -tubulins (labeled with FITC, green) were dispersed or polymerized to form filaments in the cytoplasm and cell membrane, and the CIC-3 fluorescence was partially overlapped with that of  $\alpha$ -tubulins (as shown by red dots in the overlap image). At mitotic phase of

CNE-2Z cells, the tubulins were abundantly assembled to form spindle apparatus. The overlaps of CIC-3 and microtubule were near the centrosome at the metaphase of mitosis (shown as  $M_1$  in Fig. 5), whereas at the telophase of mitosis when microtubules began to be formed in the cell membrane (shown as  $M_2$  in Fig. 5), the overlaps of CIC-3 and microtubules appeared in the cell membrane and cleavage furrow.

In the CNE-2Z cells treated with 10  $\mu$ M paclitaxel for 3 h, microtubules were highly and stably polymerized, and were mainly located in the cell membrane (Fig. 5). The expression of CIC-3 proteins was up-regulated, and the proteins formed filaments intercrossing like a bird nest in the paclitaxel-treated cells (Fig. 4). As shown in the overlap image in Fig. 5 (indicated by the red dots in the image) and in the 3D videos in the supplement (Supplementary movies 3, 4 & 5), CIC-3 proteins were partially

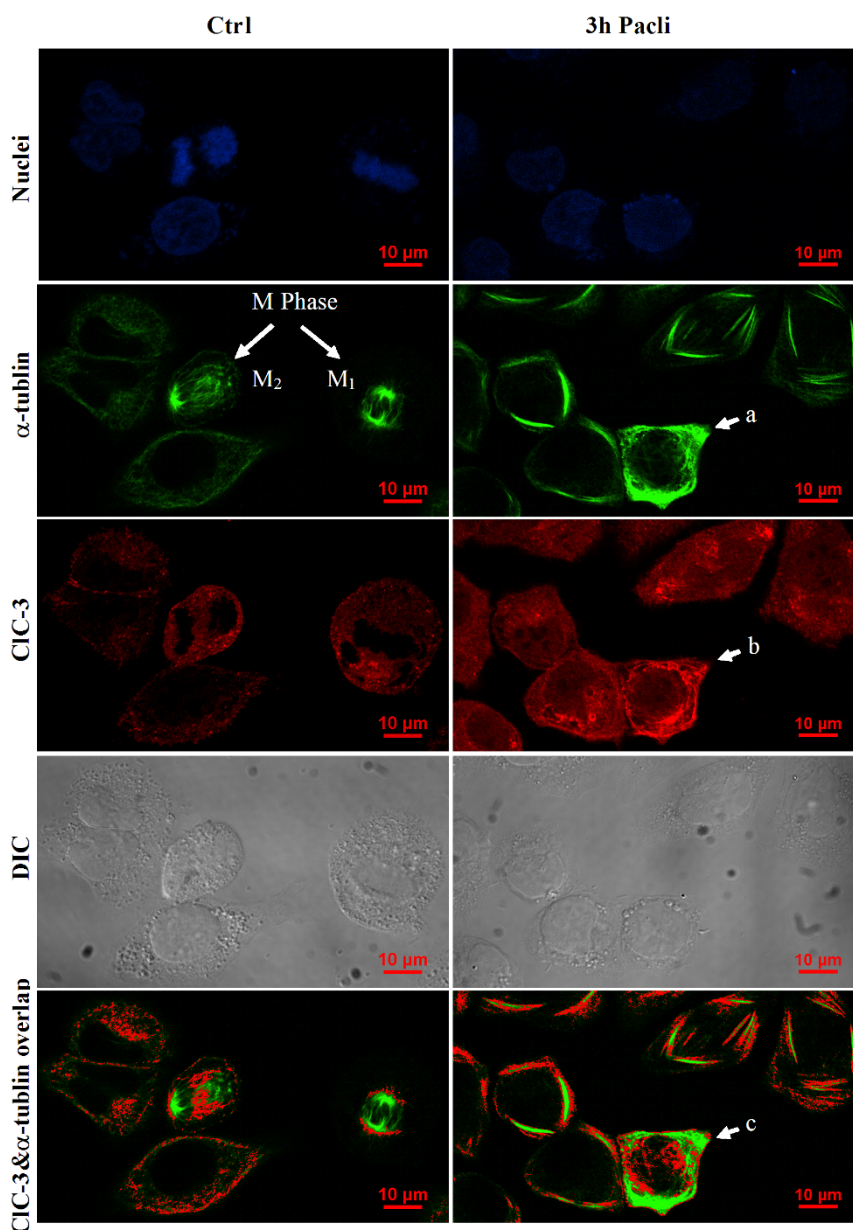


**Figure 5 | Colocalization of CIC-3 and  $\alpha$ -tubulin in normal and early apoptotic CNE-2Z cells.** The columns *Ctrl* and *3 h Pacli* show the colocalization of  $\alpha$ -tubulins and CIC-3 proteins in the control cells and the cells treated with 10  $\mu$ M paclitaxel for 3 h, respectively. **Nuclei**, cell nucleus images stained by the DNA dye DAPI (blue);  **$\alpha$ -tubulin**,  $\alpha$ -tubulin immunofluorescence labeled with FITC (green);  **$M_1$** , cell at the metaphase of mitosis;  **$M_2$** , cell at the telophase of mitosis; **CIC-3**, CIC-3 immunofluorescence labeled with cy-3 (red); **DIC**, the images obtained by differential interference contrast microscopy; **CIC-3 &  $\alpha$ -tubulin overlap**, partial overlap (shown by red dots) between CIC-3 and  $\alpha$ -tubulin. The 3D images of the paclitaxel-treated CNE-2Z cell arrowed by (a), (b) and (c) were displayed in Supplementary movie 3, Supplementary movie 4 and Supplementary movie 5 in the supplement, respectively.

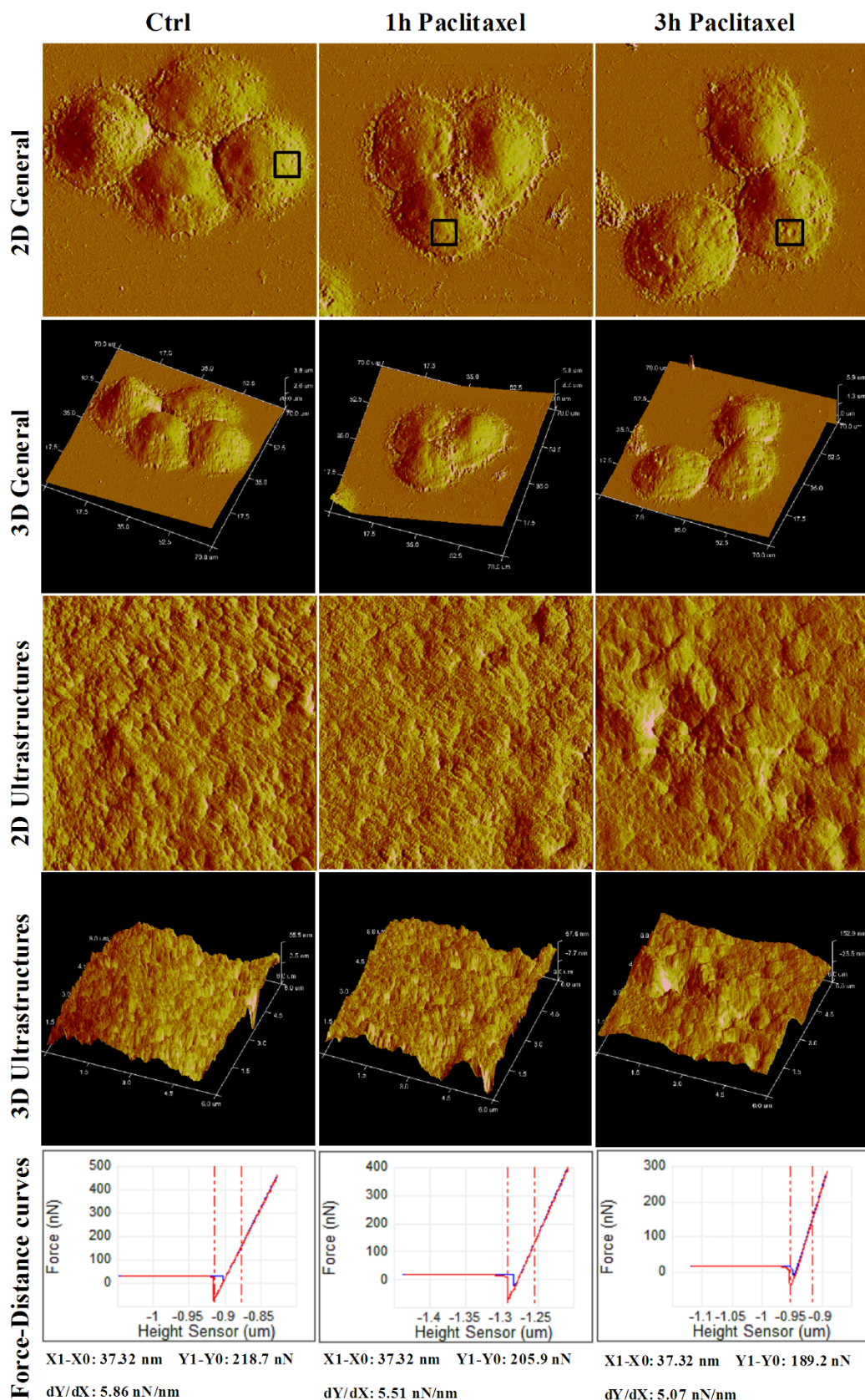


**Figure 6 | Effects of Paclitaxel on the ultrastructure of the cell membrane in CNE-2Z cells.** The atomic force microscopy (AFM) was used to detect the ultrastructure and flexibility of the cell membrane after CNE-2Z cells were incubated in 10  $\mu\text{M}$  paclitaxel for 1 h or 3 h. In the low resolution 2D or 3D whole-cell images (2D or 3D general), no noticeable changes were observed on the surface of the cells treated with paclitaxel for 1 h or 3 h. In the high resolution 2D and 3D ultrastructure images (6  $\mu\text{m} \times 6 \mu\text{m}$  patches in the black square of whole-cell images), the surface of the cells treated with paclitaxel for 1 h and 3 h became rougher, and the flexibility of the cell membrane was lower than that of control cells, presented by the Force-Distance curves.



**Table 2 | Measurements of Rq, Ra, Mean Ht and Ramps of force-distance curves in different treatments by the atomic force microscopy (Mean  $\pm$  SE, n = 3)**

Group	Rq (nm)	Ra (nm)	Mean Ht (nm)	Ramps of force- distance curves (nN/nm)
<b>Control</b>	9.73 $\pm$ 0.37	7.43 $\pm$ 0.26	6.51 $\pm$ 0.45	5.92 $\pm$ 0.02
<b>1 h Paclitaxel</b>	13.21 $\pm$ 1.53 <sup>a,**</sup>	10.42 $\pm$ 1.17 <sup>a,**</sup>	10.01 $\pm$ 0.53 <sup>a,**</sup>	5.52 $\pm$ 0.02 <sup>a,**</sup>
<b>3 h Paclitaxel</b>	39.53 $\pm$ 5.40 <sup>b,**</sup>	31.22 $\pm$ 4.64 <sup>b,**</sup>	18.40 $\pm$ 1.58 <sup>b,**</sup>	5.16 $\pm$ 0.03 <sup>b,**</sup>

<sup>\*\*</sup>*P* < 0.01;  
<sup>a</sup>vs Control;  
<sup>b</sup>vs Control or 1 h Paclitaxel. Rq, root-mean-square roughness;  
 Ra, average roughness; Mean Ht, mean height of particles.

overlapped with the microtubules assembled from  $\alpha$ -tubulins in distribution, especially in the cell membrane. Considering that the chloride currents were increased by paclitaxel, it is speculated that the microtubule cytoskeleton may participate in the trafficking of ClC-3 proteins and the microtubule cytoskeleton in the membrane may regulate ClC-3 channel activities.

**The plasma membrane became rougher and less flexible in the early apoptotic stage of CNE-2Z cells induced by paclitaxel.** The above results indicated that paclitaxel could induce the accumulation of microtubules and ClC-3 proteins in the cell membrane. These paclitaxel-induced changes may alter the structure of the membrane. To study further, the ultrastructures and flexibility of the cell membrane were detected by the atomic force microscope (AFM).

As shown in Fig. 6 and Table 2, the surface of CNE-2Z cells treated with 10  $\mu$ M paclitaxel for 1 h or 3 h did not show appreciable changes in 2D general images. In 3D general images, the control cells were plump, but the cells treated with paclitaxel seem to be depressed. In the ultrastructure images of the patches of 6  $\mu$ m  $\times$  6  $\mu$ m, Rq (root-mean-square roughness), Ra (average roughness) and Mean Ht (mean height of particles), which could evaluate the roughness of cell surface, were measured. The surface of the cells treated with paclitaxel for 1 h became rougher, indicated by the higher values in Rq, Ra and Mean Ht (*P* < 0.01, vs control). Extending the incubation time in the paclitaxel solution to 3 h, the cell membrane became much rougher, and the values of Rq, Ra and Mean Ht were much higher than those in the control and 1 h paclitaxel groups (*P* < 0.01). Force-Distance curves showed that the membrane flexibility of paclitaxel-treated cells became lower and lower along with the increase of incubation time (*P* < 0.01).

## Discussion

Recent studies have shown that abnormal expression and/or activity of a number of ion channels, including voltage-gated K<sup>+</sup>, Na<sup>+</sup>, Ca<sup>2+</sup> and TRP channels and epithelial Na<sup>+</sup>/degenerin family of ion channels, are involved in the growth/proliferation, migration and/or invasion of cancer cells. Ion channels may become potential targets for the diagnosis, prognosis and, importantly, therapy of cancer<sup>22,23,30,31</sup>. Our previous studies and the data reported by others demonstrated that the expression and activities of chloride channels were up-regulated and were cell cycle-dependent; the channels played important roles in regulation of cell cycle process, cell proliferation, migration and apoptosis, especially in the cancerous cells<sup>8,10,13,14,17,18,26,27,32–39</sup>. These data suggest that chloride channels may be a promising target of anticancer drugs.

Paclitaxel is a broad-spectrum anticancer drug, but its exact action mechanisms have not yet been clarified although much evidence has proved its action on microtubules. In this study, it was proved that paclitaxel could induce apoptosis of the nasopharyngeal carcinoma CNE-2Z cells, and this effect could be inhibited by the chloride channel blocker NPPB. The inhibition of paclitaxel-induced apoptosis by the chloride channel blocker implies that chloride channels may be a critical target of paclitaxel in its anticancer action. This was

confirmed by our further experiments. It was found that extracellular application of paclitaxel activated a chloride current with the properties similar to those of the volume-activated chloride current.

ClC-3 has been proved to be a main component of background chloride channels and mediates the process of regulatory volume decrease induced by hypotonic challenges in CNE-2Z cells<sup>27,40</sup>. To investigate the role of ClC-3 in the action of the paclitaxel-induced chloride current, we utilized ClC-3-siRNA to interfere ClC-3 protein expression in CNE-2Z cells; then the effect of the knockdown of ClC-3 expression on the activation of the current was observed. In the cells successfully transfected with ClC-3-siRNA, the chloride current was hardly induced by paclitaxel, suggesting that the ClC-3 protein may be the right chloride channel mediating the paclitaxel-induced chloride current.

Our further experiments demonstrated that paclitaxel not only activated chloride channels, but also up-regulated the expression of ClC-3 proteins. After CNE-2Z cells were treated with 10  $\mu$ M paclitaxel for 3 h, the expression of ClC-3 proteins was obviously increased. In addition, it was found that ClC-3 proteins were accumulated in the cell membrane to form intercrossed filaments like a bird nest, which was observed by virtue of the confocal scanning laser tomography and the 3D image reconstruction technology.

Paclitaxel as a microtubular stabilizing drug can cause hyper-polymerization of  $\alpha/\beta$ -tubulin heterodimers to form microtubules. It was shown in this study that elegant changes of the microtubule cytoskeleton appeared in different cell cycle phases of control CNE-2Z cells. The fluorescence of ClC-3 and that of tubulin were partially overlapped. In the cells treated with paclitaxel, tubulins were highly and stably polymerized, and were mainly located in the cell membrane. Interestingly, along with the translocation of tubulins and the increased overlap between ClC-3 proteins and tubulins, the distribution of ClC-3 proteins in the cell membrane was also increased significantly. The data imply that there is a close relationship between ClC-3 proteins and the microtubule cytoskeleton. Much of published work has disclosed that the interaction between ion channels and the actin-based cytoskeleton in epithelial cells not only plays a role in maintaining the polarized distribution of ion channels within specific membrane domains, but also functions in the intracellular trafficking and regulation of channel activity<sup>41</sup>. The dynamic turnover of microtubule cytoskeleton allows cell to reorganize an array of microtubules rapidly for cell polarity, motility, mitosis and vesicle traffic<sup>42</sup>. The study of the relationship between TRP channels and microtubule cytoskeleton demonstrates that the activity of TRP channels is regulated by microtubular structures, and TRP channels bind dynamically to intact microtubules but not to tubulin dimmers<sup>28,29,43,44</sup>. Based on the above data, we speculate that microtubules may facilitate the trafficking of ClC-3 proteins and the ClC-3 channel activity; the long lasting opening of microtubule-linked ClC-3 channels induced by paclitaxel results in apoptosis of CNE-2Z cells.

Moreover, changes in the ultrastructure and flexibility of the cell membrane were observed by the atomic force microscopy in the early stage of apoptosis induced by paclitaxel. These changes may be the



featured phenomena of early apoptosis. However, it is unclear whether these changes are associated with CIC-3. Our previous works showed that the hypotonicity-induced changes of membrane ultrastructures in CNE-2Z cells were associated with the modulation of chloride channels<sup>35</sup>. In this study, it was observed that both tubulin and the chloride channel protein CIC-3 were accumulated in the cell membrane to form the microtubule skeleton and intercrossed filaments. There might be a possibility that the changes in the ultrastructure and the decrease of flexibility could result from the changes of CIC-3 and tubulin in arrangement and distribution in the cell membrane. However, to clarify their relationships, more future work should be done.

In conclusion, the volume-sensitive chloride channel may be a critical target of paclitaxel in its anticancer action. CIC-3 proteins play a pivotal role in the activation of the paclitaxel-induced chloride current. Microtubules may facilitate the CIC-3 channel activity and may be associated with the trafficking of CIC-3 proteins. The microtubule-associated CIC-3 may be involved in the regulation of paclitaxel-induced CNE-2Z cells apoptosis. The up-regulation of CIC-3 and its accumulation with microtubules in the cell membrane to form intercrossed filaments may be one of the factors causing the cell membrane changes in paclitaxel-induced apoptosis.

## Methods

**Cell culture and siRNA transfection.** The poorly differentiated nasopharyngeal carcinoma CNE-2Z cells were routinely grown in RPMI 1640 medium with 10% newborn calf serum, 100 IU/ml penicillin and 100 µg/ml streptomycin in the atmosphere of saturated humidity with 5% CO<sub>2</sub> and 95% O<sub>2</sub> at 37°C. The cells were digested by trypsinization and subcultured every 2 days.

CNE-2Z cells were seeded in 6-well culture plates and transfected with siRNA when cells were 30% ~ 50% confluences. The siRNA in the final concentration of 100 nM was transfected into CNE-2Z cells by Lipofectamine<sup>TM</sup>2000 (Invitrogen, USA) following the manufacturer's instructions. The siRNA was obtained by chemical synthesis by the GenePharma Company (China). The sense strand of CIC-3-siRNA was 5'-CAAUGGAUUCCUGUCAUAtt-3', and the sense strand of negative control siRNA (NC-siRNA) was 5'-UUCUCCGAACGUGUCACGUTT-3'.

**Antibodies, chemicals and solutions.** Antibodies of CIC-3 (ab86192), cleaved caspase-3 (9661S),  $\alpha$ -tubulin (AT819) and  $\beta$ -actin (BM0672) were bought from Abcam (USA), Cell Signaling Technology (USA), Beyotime (China) and BOSTER (China), respectively. Annexin V-FITC/PI apoptosis detection kit (PF032) was bought from Merck (Germany). All other chemicals were purchased from Sigma (USA). Paclitaxel (T7191), 5-Nitro-2-(3-phenylpropylamino) benzoic acid (NPPB, N4779) and 4, 4'-Diisothiocyanatostilbene-2, 2'-disulfonic acid disodium salt hydrate (DIDS, D3514) were prepared as stocking solutions in dimethyl sulfoxide and diluted to final concentrations using bath solutions.

The isotonic bath solution contained (in mM) 70 NaCl, 0.5 MgCl<sub>2</sub>, 2 CaCl<sub>2</sub>, 10 HEPES and 140 D-mannitol. The hypotonic bath solution (47% hypotonic) was obtained by omitting D-mannitol from the isotonic solution. The hypertonic bath solution (47% hypertonic) was prepared by adding 140 mM D-mannitol into isotonic solution. The pipette solution contained (in mM) 70 NMDG-Cl, 1.2 MgCl<sub>2</sub>, 10 HEPES, 1 EGTA, 140 D-mannitol and 2 ATP. The pH of bath and pipette solutions was adjusted to 7.40 and 7.25 with Tris-base, respectively.

**Detection of apoptosis by Annexin V-FITC and PI.** Annexin V-FITC in cooperation with propidium iodide (PI) is usually used to detect the early and late apoptotic cells<sup>45</sup>. In this study, the Annexin V-FITC/PI double staining assay was employed to detect paclitaxel-induced apoptosis. Annexin V-FITC and PI were diluted with 1 × Binding Buffer to the concentrations of 0.5 µg/ml and 0.6 µg/ml, respectively. The cells on culture plates were washed with pre-cold PBS for 3 times, bathed in 0.5 µg/ml Annexin V-FITC solution for 15 min and in 0.6 µg/ml PI solution for 5 min, and then rinsed with 1 × Binding Buffer for 3 times. The fluorescent images of cells in different groups were captured by the Nikon C1-si confocal microscope (Japan) using the same capturing parameters, and the early and late apoptotic cells were analyzed. In analyzing cell images, the software function "Lookup Tables (LUTs)" was enabled to obtain enhanced fluorescent cell images.

**Chloride current recordings.** The coverslip with CNE-2Z cells was put in a bath chamber and whole-cell Cl<sup>-</sup> currents were recorded with 4 ~ 6 M $\Omega$  pipettes and EPC-7 patch clamp amplifier (Heka, Germany) at 20 ~ 24°C. The membrane potential was held at the Cl<sup>-</sup> equilibrium potential (0 mV) and stepped to 0,  $\pm$  40 and  $\pm$  80 mV for 200 ms repeatedly, with a 4 s interval between pulses. Currents were measured at 10 ms after onset of voltage steps. Electrophysiological signals were recorded with a sampling rate of 3 kHz, and filtered by two steps (filter 1, 10 kHz; filter 2, 3 kHz) and stored in a computer via a 1401 interface (CED, Cambridge

Electronic Design, UK). The data were collected and analyzed using the EPC software package (CED, Cambridge Electronic Design, UK).

**Immunofluorescence.** CNE-2Z cells were briefly washed in PBS, and then fixed for 15 min in 4% paraformaldehyde. After rinsing cells 6 times with PBS, cells were permeated with 0.5% Triton X-100 for 5 min, blocked with 10% sheep serum for 45 min, incubated in 1% sheep serum solutions containing primary antibodies (1 : 100 for cleaved caspase-3,  $\alpha$ -tubulin and CIC-3) overnight at 4°C, washed with PBS to remove unbound primary antibodies, and then soaked in 1% sheep serum solutions containing secondary antibodies labeled with cy-3 or FITC for 1 h at 37°C. After the unbound antibodies were washed away, the coverslips were inverted onto the mounting medium on glass slides, sealed with nail varnish, and examined under the Nikon C1-si confocal microscope (Japan).

**Western blotting.** CNE-2Z cells were lysed with RIPA lysis buffer. The collected total proteins were quantified by BCA protein assay and boiled with the loading buffer for 5 min to denature the proteins. The proteins (40 µg) were loaded onto 12% SDS-PAGE gel, separated, transferred onto nitrocellulose membrane, blocked in 5% non-fat dry milk for 1 h at 37°C, soaked in the TBST solutions containing primary antibodies (1 : 1500 for CIC-3 and 1 : 1000 for  $\beta$ -actin) overnight at 4°C, rinsed with TBST solutions to remove unbound primary antibodies, and then exposed to the TBST solutions containing secondary antibodies labeled with peroxidase for 1 h at 37°C. After the unbound antibodies were washed away, the chemiluminescent detection method was used to detect the target proteins.

**Detection of membrane ultrastructure.** The atomic force microscopy (AFM) is a type of scanning probe microscopy with a demonstrated resolution of fractions of a nanometer. In current study, the ultrastructures of the cell membrane were detected by an atomic force microscope (Bioscope Catalyst NanoScope-V, Veeco instruments, USA) at 20 ~ 24°C. AFM probes (Budget Sensors, Bulgaria) with resonance frequency 150 kHz and spring constant 5 N/m were used and the scan rate was 0.4 Hz. The force-distance curves were performed. The following parameters were used: Sens. DeflSens 17.50 nm/V, Spring Constant 6.651 N/m and Effective BW 2105 Hz.

CNE-2Z cells were seeded on the coverslips in 6-well culture plates, grown overnight, and then bathed in the RPMI 1640 medium with or without 10 µM paclitaxel for 1 or 3 h. Cells were washed three times with PBS, fixed for 15 min in 4% paraformaldehyde, washed three times with pure water and then dried in air. The membrane ultrastructures of the control cells and the cells treated with paclitaxel for 1 h and 3 h were detected by AFM. The Rq (root-mean-square roughness), Ra (average roughness) and Mean Ht (mean height of particles) and the ramps of force-distance curves were analyzed with NanoScope Analysis software (Version 1.2, Veeco instruments, USA).

**Statistics.** An analysis of variance (ANOVA) (SPSS, Chicago, USA) was used to test for significant differences and differences were considered significant at  $P < 0.05$ . Data were expressed as mean  $\pm$  standard error (SE).

- Rowinsky, E. K. The development and clinical utility of the taxane class of antimicrotubule chemotherapy agents. *Annu. Rev. Med.* **48**, 353–374 (1997).
- Wang, T. H., Wang, H. S. & Soong, Y. K. Paclitaxel-induced cell death: where the cell cycle and apoptosis come together. *Cancer* **88**, 2619–2628 (2000).
- Smotter, M. *et al.* The role of Tau protein in resistance to paclitaxel. *Cancer Chemoth. Pharm.* **68**, 553–557 (2011).
- Mroz, P., Yaroslavsky, A., Kharkwal, G. B. & Hamblin, M. R. Cell Death Pathways in Photodynamic Therapy of Cancer. *Cancers* **3**, 2516–2539 (2011).
- Bortner, C. D., Scoltock, A. B., Sifre, M. I. & Cidlowski, J. A. Osmotic stress resistance imparts acquired anti-apoptotic mechanisms in lymphocytes. *J. Biol. Chem.* **287**, 6284–6295 (2012).
- Shimizu, T., Maeno, E. & Okada, Y. Prerequisite role of persistent cell shrinkage in apoptosis of human epithelial cells. *Acta physiol. Sin.* **59**, 512–516 (2007).
- Ernest, N. J., Habela, C. W. & Sontheimer, H. Cytoplasmic condensation is both necessary and sufficient to induce apoptotic cell death. *J. Cell Sci.* **121**, 290–297 (2008).
- Maeno, E., Ishizaki, Y., Kanaseki, T., Hazama, A. & Okada, Y. Normotonic cell shrinkage because of disordered volume regulation is an early prerequisite to apoptosis. *P. Natl. Acad. Sci. U SA.* **97**, 9487–9492 (2000).
- Bortner, C. D. & Cidlowski, J. A. Cell shrinkage and monovalent cation fluxes: role in apoptosis. *Arch. Biochem. Biophys.* **462**, 176–188 (2007).
- Stutzin, A. & Hoffmann, E. K. Swelling-activated ion channels: functional regulation in cell-swelling, proliferation and apoptosis. *Acta. Physiol.* **187**, 27–42 (2006).
- Valencia-Cruz, G. *et al.* K(bg) and Kv1.3 channels mediate potassium efflux in the early phase of apoptosis in Jurkat T lymphocytes. *Am. J. Physiol.-Cell Ph.* **297**, C1544–1553 (2009).
- Bortner, C. D. & Cidlowski, J. A. The role of apoptotic volume decrease and ionic homeostasis in the activation and repression of apoptosis. *Pflugers Arch.* **448**, 313–318 (2004).
- Hernandez-Enriquez, B., Arellano, R. O. & Moran, J. Role for ionic fluxes on cell death and apoptotic volume decrease in cultured cerebellar granule neurons. *Neuroscience* **167**, 298–311 (2010).



14. Lang, F. *et al.* Ion channels and cell volume in regulation of cell proliferation and apoptotic cell death. *Contrib. Nephrol.* **152**, 142–160 (2006).
15. Qian, Y. *et al.* ClC-3 chloride channel prevents apoptosis induced by hydrogen peroxide in basilar artery smooth muscle cells through mitochondria dependent pathway. *Apoptosis* **16**, 468–477 (2011).
16. Zhang, H. N., Zhou, J. G., Qiu, Q. Y., Ren, J. L. & Guan, Y. Y. ClC-3 chloride channel prevents apoptosis induced by thapsigargin in PC12 cells. *Apoptosis* **11**, 327–336 (2006).
17. Bozeat, N. D. *et al.* Activation of Volume Regulated Chloride Channels Protects Myocardium from Ischemia/reperfusion Damage in Second-window Ischemic Preconditioning. *Cell Physiol. Biochem.* **28**, 1265–1278 (2011).
18. Cheng, G., Shao, Z., Chaudhari, B. & Agrawal, D. K. Involvement of chloride channels in TGF-beta1-induced apoptosis of human bronchial epithelial cells. *Am. J. Physiol.-Lung C.* **293**, L1339–L1347 (2007).
19. Scabini, M. *et al.* In vivo imaging of early stage apoptosis by measuring real-time caspase-3/7 activation. *Apoptosis* **16**, 198–207 (2011).
20. Salvesen, G. S. Caspases: opening the boxes and interpreting the arrows. *Cell Death Differ.* **9**, 3–5 (2002).
21. Ghavami, S. *et al.* Apoptosis and cancer: mutations within caspase genes. *J. Med. Genet.* **46**, 497–510 (2009).
22. Arcangeli, A., Pillozzi, S. & Becchetti, A. Targeting ion channels in leukemias: a new challenge for treatment. *Curr. Med. Chem.* **19**, 683–696 (2012).
23. Arcangeli, A. *et al.* Targeting ion channels in cancer: a novel frontier in antineoplastic therapy. *Curr. Med. Chem.* **16**, 66–93 (2009).
24. Xiao-ya, Y. *et al.* Chloride currents activated by cisplatin in nasopharyngeal carcinoma cells. *Chin. J. Pathophysiol.* **25**(4), 666–669 (2009).
25. Min, X. J. *et al.* Dysfunction of volume-sensitive chloride channels contributes to cisplatin resistance in human lung adenocarcinoma cells. *Exp. Biol. Med.* **236**, 483–491 (2011).
26. Chen, L. *et al.* Cell cycle-dependent expression of volume-activated chloride currents in nasopharyngeal carcinoma cells. *Am. J. Physiol.-Cell Ph.* **283**, C1313–C1323 (2002).
27. Zhu, L. *et al.* Differential expression and roles of volume-activated chloride channels in control of growth of normal and cancerous nasopharyngeal epithelial cells. *Biochem. Pharmacol.* **83**, 324–334 (2012).
28. Li, Q. *et al.* Polycystin-2 cation channel function is under the control of microtubular structures in primary cilia of renal epithelial cells. *J. Biol. Chem.* **281**, 37566–37575 (2006).
29. Montalbetti, N., Li, Q., Wu, Y., Chen, X. Z. & Cantiello, H. F. Polycystin-2 cation channel function in the human syncytiotrophoblast is regulated by microtubular structures. *J. Physiol.* **579**, 717–728 (2007).
30. Li, M. & Xiong, Z. G. Ion channels as targets for cancer therapy. *Int. J. Physiol. Pathophysiol. Pharmacol.* **3**, 156–166 (2011).
31. Fraser, S. P. & Pardo, L. A. Ion channels: functional expression and therapeutic potential in cancer. Colloquium on Ion Channels and Cancer. *EMBO Rep.* **9**, 512–515 (2008).
32. Mao, J. *et al.* Cell cycle-dependent subcellular distribution of ClC-3 in HeLa cells. *Histochem. Cell Biol.* **137**, 763–776 (2012).
33. Cao, G. *et al.* Volume-sensitive chloride channels are involved in maintenance of basal cell volume in human acute lymphoblastic leukemia cells. *J. Membrane Biol.* **240**, 111–119 (2011).
34. Yang, L. *et al.* Uncoupling of K<sup>+</sup> and Cl<sup>-</sup> transport across the cell membrane in the process of regulatory volume decrease. *Biochem. Pharmacol.* **84**, 292–302 (2012).
35. Bai, Z. *et al.* Lithium inhibits cell volume regulation by acting on chloride channels and modifies ultrastructures of the cell membrane in nasopharyngeal carcinoma cells. *Eur. J. Pharmacol.* **641**, 88–95 (2010).
36. Mao, J. *et al.* Tamoxifen inhibits migration of estrogen receptor-negative hepatocellular carcinoma cells by blocking the swelling-activated chloride current. *J. Cell. Physiol.* **228**(5), 991–1001 (2013).
37. Mao, J. *et al.* Suppression of ClC-3 channel expression reduces migration of nasopharyngeal carcinoma cells. *Biochem. Pharmacol.* **75**, 1706–1716 (2008).
38. Zhang, H. *et al.* The ClC-3 chloride channel protein is a downstream target of cyclin D1 in nasopharyngeal carcinoma cells. *Int. J. Biochem. Cell Biol.* **45**, 672–683 (2013).
39. Okada, Y. *et al.* Volume-sensitive chloride channels involved in apoptotic volume decrease and cell death. *J. Membrane Biol.* **209**, 21–29 (2006).
40. Yang, L. *et al.* ClC-3 is a main component of background chloride channels activated under isotonic conditions by autocrine ATP in nasopharyngeal carcinoma cells. *J. Cell. Physiol.* **226**, 2516–2526 (2011).
41. Mazzochi, C., Benos, D. J. & Smith, P. R. Interaction of epithelial ion channels with the actin-based cytoskeleton. *Am. J. Physiol.-Renal* **291**, F1113–F1122 (2006).
42. Cassimeris, L. *et al.* Fueled by microtubules: does tubulin dimer/polymer partitioning regulate intracellular metabolism? *Cytoskeleton* **69**, 133–143 (2012).
43. Goswami, C. TRPV1-tubulin complex: involvement of membrane tubulin in the regulation of chemotherapy-induced peripheral neuropathy. *J. Neurochem.* **123**, 1–13 (2012).
44. Storti, B., Bizzarri, R., Cardarelli, F. & Beltram, F. Intact microtubules preserve transient receptor potential vanilloid 1 (TRPV1) functionality through receptor binding. *J. Biol. Chem.* **287**, 7803–7811 (2012).
45. van Engeland, M., Nieland, L. J., Ramaekers, F. C., Schutte, B. & Reutelingsperger, C. P. Annexin V-affinity assay: a review on an apoptosis detection system based on phosphatidylserine exposure. *Cytometry* **31**, 1–9 (1998).

## Acknowledgments

This work was supported by the National Natural Science Foundation of China (30771106, 30870567, 30871267, U0932004/L02, 90913020, 31070997, 81173064, 81272223, 81273539), the Natural Science Foundation of Guangdong Province (S2011010001589) and the Specialized Research Fund for the Doctoral Program of Higher Education (20124401110009).

## Author contributions

H.Z. and H.L. prepared the main figures and the main manuscript text. L.Y., Z.D., H.L., D.Y., Z.B. and L.Z. co-prepared figure 1, S1, S2 and S4. L.C., L.W. and W.Y. designed and supervised this study, and prepared the manuscript.

## Additional information

**Supplementary information** accompanies this paper at <http://www.nature.com/scientificreports>

**Competing financial interests:** The authors declare no competing financial interests.

**How to cite this article:** Zhang, H. *et al.* The ClC-3 chloride channel associated with microtubules is a target of paclitaxel in its induced-apoptosis. *Sci. Rep.* **3**, 2615; DOI:10.1038/srep02615 (2013).



This work is licensed under a Creative Commons Attribution-NonCommercial-ShareAlike 3.0 Unported license. To view a copy of this license, visit <http://creativecommons.org/licenses/by-nc-sa/3.0>